# In-plane anisotropy of the hole $g$ factor in CdTe/(Cd,Mg)Te quantum wells studied by spin-dependent photon echoes

S. V. Poltavtsev,[1,2,*] I. A. Yugova,[3] A. N. Kosarev,[1,4] D. R. Yakovlev,[1,4] G. Karczewski,[5] S. Chusnutdinow,[5] T. Wojtowicz,[6] I. A. Akimov,[1,4] and M. Bayer[1,4]

[1]*Experimentelle Physik 2, Technische Universität Dortmund, 44221 Dortmund, Germany*
[2]*Spin Optics Laboratory, Saint Petersburg State University, 198504 Saint Petersburg, Russia*
[3]*Physics Faculty, Saint Petersburg State University, 199034 Saint Petersburg, Russia*
[4]*Ioffe Institute, Russian Academy of Sciences, 194021 Saint Petersburg, Russia*
[5]*Institute of Physics, Polish Academy of Sciences, PL-02668 Warsaw, Poland*
[6]*International Research Centre MagTop, Institute of Physics, Polish Academy of Sciences, PL-02668 Warsaw, Poland*

(Received 10 February 2020; revised manuscript received 5 April 2020; accepted 13 April 2020; published 12 May 2020)

Optical control of spins in condensed matter systems such as semiconductor nanostructures requires precise knowledge of the polarization properties of the associated optical transitions subject to an external magnetic field. Here, we demonstrate that coherent optical spectroscopy in the form of photon echoes can be successfully used to evaluate the magnetic anisotropies of valence-band states. It manifests in drastic changes of the transient signals when the orientation of the magnetic field with respect to the crystallographic axes is varied. In particular, we use the two-pulse spin-dependent photon echo to study the in-plane hole spin anisotropy in a 20-nm-thick $CdTe/Cd_{0.76}Mg_{0.24}Te$ single quantum well by exciting the donor-bound exciton resonance. We take advantage of the photon echo sensitivity to the relative phase of the electron and hole spin precession in the ground and excited states, respectively, and study various interactions contributing to the hole in-plane spin properties. The main contribution is found to arise from the crystal cubic symmetry described by the Luttinger parameter $q = 0.095 \pm 0.005$, which is substantially larger than the one theoretically expected for CdTe or found in other quantum well structures. Another contribution is induced by the strain within the quantum well. These two contributions lead to different harmonics of the spin precession frequencies in the photon echo experiment, when the strength and orientation of the Voigt magnetic field are varied. The magnitude of the effective in-plane hole $g$ factor is found to vary in the range $|\tilde{g}_h|$=0.125–0.160 in the well plane.

DOI: 10.1103/PhysRevResearch.2.023160

## I. INTRODUCTION

Once the magneto-optical properties of a condensed matter system become relevant, a detailed knowledge of the spin level structure of the electronic states involved in optical transitions is essential. Particularly in semiconductors, for manipulating an optically excited state in a quantum well (QW) or in a quantum dot (QD), the properties of the hole angular momentum must be taken into account. Due to the strong spin-orbit interaction, the structure of the valence-band states is complex and, as a consequence, also the hole $g$ factor is strongly anisotropic [1]. In the magnetic field this is manifested in an anisotropic Zeeman splitting. Here, the configuration in which the magnetic field is applied perpendicular to the light wave vector (and to the structure quantization axis), for which the intrinsic optical transitions become linearly polarized, is especially interesting. In the isotropic case, the optical transitions split by the field would be polarized either along or perpendicular to the magnetic field axis as for atomic systems [2]. However, in a solid state, the effective magnetic field, acting on the holes, does not coincide with the external magnetic field. This is because confinement and strain significantly modify the valence-band eigenstates and, as a result, change the polarization of the optical transitions [3].

There are various methods to study the hole spin in low-dimensional semiconductor systems. Some of them, such as polarized photoluminescence [4–6] and spin-flip Raman scattering [7–9], require the application of quite strong transverse magnetic fields in order to resolve the small Zeeman splittings, by which also band mixing effects are changed, for example. Additionally, tilting of the field axis away from the Voigt geometry is often used to involve the larger out-of-plane hole $g$ factor component in the Zeeman interaction [10]. Also the spin noise technique allows studying the hole spin in certain systems with small or zero hole $g$ factor inhomogeneities such as single QDs [11]. Other methods based on pump-probe Kerr or Faraday rotation are mostly applicable to systems with

*sergei.poltavtcev@tu-dortmund.de

resident holes, because, otherwise, the hole spin precession is screened by the signal originating from the electron spin [12–14]. As a result, the possibilities to study the in-plane anisotropy of the hole spin by these methods are somewhat limited and only a few of them have been employed so far for that [8,9,15]. Moreover, the true anisotropy of electronic states induced by a magnetic field cannot be recognized in the variation of the Zeeman splitting when the magnetic field orientation is changed, but in the polarization properties of the optical transitions which have been elaborated only for photoluminescence [3]. Yet photoluminescence studies require large magnetic fields or extremely high spatial resolution in order to address single excitons suppressing, thus, the inhomogeneous broadening of the investigated systems [5].

On the other hand, time-resolved coherent optical methods allow for tracing the precise hole spin dynamics in the limit of small magnetic fields. One of these methods is four-wave mixing and especially the photon echo (PE) technique, which provides access to the homogeneous optical linewidth [16]. Recently, it was shown for various systems that photon echoes depend sensitively on the applied transverse magnetic field (see, e.g., Refs. [17,18]). In particular, the transverse hole $g$ factor can be measured using spin-dependent photon echoes [19]. Previous work demonstrated that coherent optical methods in combination with applying transverse magnetic fields open unique opportunities to study the spin properties of the electronic states in semiconductor nanostructures. However, to the best of our knowledge, none of the previous studies addressed the impact of the magnetic-field-induced anisotropy of the hole spin states on the coherent optical response.

In this paper, we investigate the in-plane anisotropy of the hole spin in a single CdTe/(Cd,Mg)Te QW, manifested through the photon echoes from the neutral exciton bound to a donor ($D^0X$) in a transverse magnetic field. The absence of the electron-hole spin-exchange interaction for the $D^0X$ complex significantly simplifies the analysis of the magnetic field dependences, providing an excellent model system to test our technique. We find that the in-plane hole $g$ factor is highly anisotropic as a result of several contributions, which strongly influence the coherent optical dynamics of $D^0X$, when the orientation of the magnetic field with respect to crystallographic axes is varied. The photon echo transients as a result of linearly polarized pulses are especially interesting. In this case the angular dependence of the signal allows one to determine the eigenpolarizations of the optical transitions which do not necessarily coincide with the direction of the external magnetic field. The latter is crucial for optical spin control in semiconductor nanostructures in magnetic field. The proposed approach can be applied for investigation of the magnetic anisotropies in semiconductor and condensed matter systems with different dimensionality from three-dimensional down to zero-dimensional (bulk, quantum well, quantum wires, and quantum dots) and is not limited to some particular material system.

## II. THEORETICAL MODEL

We start with the theoretical consideration of the magnetic-field-dependent two-pulse PE generated by the spectrally isolated, negatively charged exciton (trion) or $D^0X$ in a QW, neglecting many-body effects. The system is excited by two short laser pulses of specific polarizations ($\mathcal{P}_1$ and $\mathcal{P}_2$) and separated by their time delay $\tau$. The excitation is followed by the two-pulse PE emission delayed by $\tau$ relative to the second pulse. The PE amplitude is studied as well in a specific $\mathcal{P}_{\rm PE}$ polarization, so that the experiment can be characterized by the polarization sequence $\mathcal{P}_1\mathcal{P}_2 \rightarrow \mathcal{P}_{\rm PE}$. We use as a reference frame the one associated with the crystal axes, where $z$ || [100] is the growth direction and $x$ || [010] and $y$ || [001] are the in-plane axes, as shown in Fig. 1(a). The magnetic field is applied in the QW plane ($\mathbf{B} \perp z$) under the angle $\varphi$ with respect to the $x$ axis.

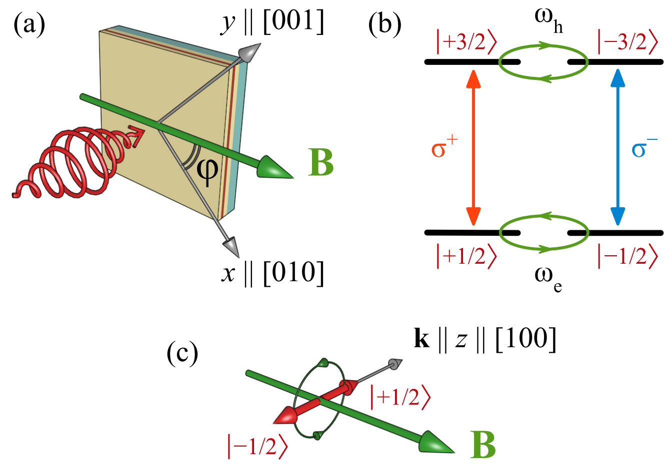


FIG. 1. Representation of experimental geometry and spin level structure in the circular polarization basis. (a) Reference frame associated with the QW structure and its orientation with respect to the magnetic field. (b) Energy-level scheme using as a basis the angular momentum states along $\mathbf{k}||z$. The numbers in brackets indicate the total angular momentum projections on the $z$ axis. (c) Electron-spin orientations in the ground states $|\pm 1/2\rangle$, which have equal energies and are mixed by the magnetic field.

### A. Circular polarization basis

The negatively charged exciton (trion) consists of two electrons and a hole, while the ground state implies a resident electron with spin 1/2. In the singlet state of $D^0X$, the two electron spins are antiparallel, so that the $D^0X$ spin state is determined by the hole spin. Both systems, the trion and donor-bound exciton, can be represented by the four-level energy scheme displayed in Fig. 1(b).

First, we consider the circular polarization basis, in which the eigenstates of total angular momentum projection on the $z$ axis correspond to the optically addressed states. The optical selection rules separate the four levels into two arms of allowed optical transitions using opposite circularly polarized light, as shown in Fig. 1(b). The electron ground states with angular momentum projections $|\pm 1/2\rangle$ have the same energy and become mixed by the in-plane magnetic field $\mathbf{B}$. This is illustrated by the sketch in Fig. 1(c). So are the excited states (trion/$D^0X$) with total angular momentum projections $|\pm 3/2\rangle$.

To describe the magnetic properties of the electron or trion/$D^0X$ states, we use the Hamiltonian in the form

$$H = \frac{\omega}{2}\begin{pmatrix} 0 & e^{-i\theta} \\ e^{i\theta} & 0 \end{pmatrix}, \tag{1}$$

where $\omega$ is the effective Larmor frequency and $\theta$ is the angle between the $x$ axis and effective magnetic field axis, around which Larmor precession occurs. Because of the anisotropy of the spin splitting, the angle $\theta$ can differ from the actual magnetic field angle $\varphi$.

For the electron in the ground state, we take the Zeeman interaction to be isotropic using the constant in-plane electron Landé factor $g_e$. The Larmor frequency of the electron is $\omega_e = g_e\mu_B B/\hbar$, where $\mu_B$ is the Bohr magneton and $\hbar$ is the Planck constant. The electron experiences the actual magnetic field, so that $\theta = \varphi_e \equiv \varphi$.

The heavy-hole spin is known to be strongly anisotropic in the QW plane [4]. Thereby, a number of interactions contributing to the effective hole $g$ factor $\tilde{g}_h$ have to be considered. We follow the theoretical approach by Semenov and Ryabchenko [3] and include the three main contributions expected to determine the hole spin dynamics: (i) the Zeeman interaction leading to a heavy-hole splitting in third order of perturbation theory given by $\omega_z = \frac{3}{2}(g_h\mu_B B)^3/\hbar\Delta_{\mathrm{LH}}^2$ [20], where $\Delta_{\mathrm{LH}}$ is the heavy-hole–light-hole (HH-LH) splitting and $g_h$ characterizes the Zeeman interaction of the hole, where the angle at which the effective magnetic field appears due to this contribution is $\theta = 3\varphi$; (ii) the (non-Zeeman) interaction due to the cubic crystal symmetry with $\omega_q = \frac{3}{2}q\mu_B B/\hbar$ and $\theta = -\varphi$, where $q$ is the Luttinger parameter [20,21]; and (iii) the strain-induced potential of $C_{2v}$ symmetry for the hole inside the QW, which mixes HH and LH states in first order of perturbation theory and provides an additional splitting $\omega_{ht} = u\mu_B B/\hbar$ with the parameter $u \sim g_h/\Delta_{\mathrm{LH}}$ and is determined by the in-plane strain axis with the angle $\phi$ relative to the $x$ axis. Summing these contributions results in the effective magnetic field angle $\theta = \varphi + 2\phi + \pi/2$ [3]. Accounting for all of them was shown to be important in self-assembled semiconductor QDs [5,6,22,23].

Including the three contributions, we write the hole spin Hamiltonian in the form

$$\begin{aligned} H_h = {} & \frac{\omega_z}{2}\begin{pmatrix} 0 & e^{-i3\varphi} \\ e^{i3\varphi} & 0 \end{pmatrix} + \frac{\omega_q}{2}\begin{pmatrix} 0 & e^{i\varphi} \\ e^{-i\varphi} & 0 \end{pmatrix} \\ & + \frac{i\omega_{ht}}{2}\begin{pmatrix} 0 & -e^{-i(\varphi+2\phi)} \\ e^{i(\varphi+2\phi)} & 0 \end{pmatrix} \equiv \frac{\omega_h}{2}\begin{pmatrix} 0 & e^{-i\varphi_h} \\ e^{i\varphi_h} & 0 \end{pmatrix}. \end{aligned} \tag{2}$$

The effective hole precession frequency $\omega_h = \tilde{g}_h\mu B/\hbar$ obtained in Appendix A 2 from this Hamiltonian is given by

$$\begin{aligned} \omega_h &= \sqrt{N^2 + M^2}, \\ N &= \omega_z\cos(3\varphi) + \omega_q\cos(\varphi) - \omega_{ht}\sin(\varphi + 2\phi), \\ M &= \omega_z\sin(3\varphi) - \omega_q\sin(\varphi) + \omega_{ht}\cos(\varphi + 2\phi). \end{aligned} \tag{3}$$

The angle of the effective magnetic field experienced by the hole $\theta = \varphi_h$ can be found from $\tan(\varphi_h) = M/N$.

As a result, we find for the PE amplitude, analyzed in the polarization chosen to be identical to that of the first pulse ($\mathcal{P}_{\mathrm{PE}} = \mathcal{P}_1$), for which the strongest and most informative PE signals are expected,

$$P_{\sigma^+\sigma^\pm\to\sigma^+} \propto [1 \pm \cos(\omega_e\tau)][1 \pm \cos(\omega_h\tau)]. \tag{4}$$

Hereafter, we fix the pulse delay $\tau$ and scan the magnetic field amplitude $B$, which allows us to neglect any relaxation processes in the coherent dynamics of the system. As a result, the effective Larmor frequencies $\omega_i$ are not constants in our consideration, but rather change with the magnetic field strength $B$, in accordance with the interactions (i)–(iii).

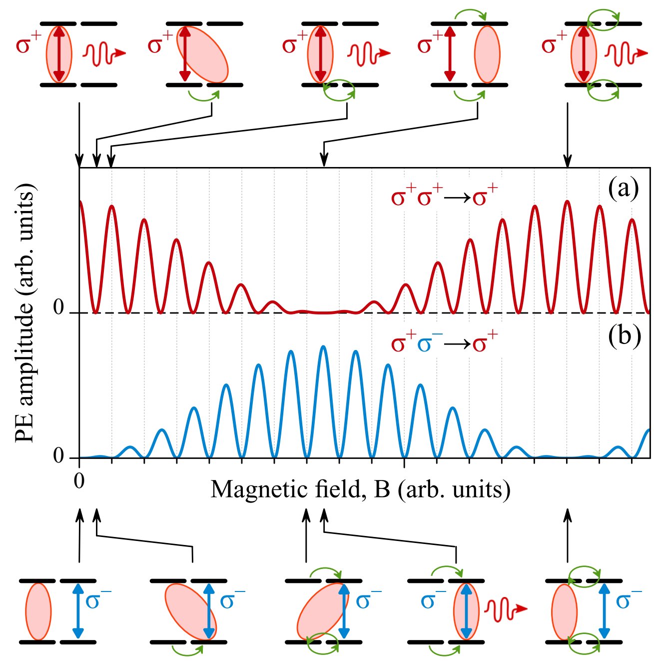


FIG. 2. Magnetic field dependences of the PE amplitude calculated for the circularly (a) co-polarized and (b) cross-polarized configurations using Eq. (4) for $|g_e| = 15|\tilde{g}_h|$ and a fixed delay $\tau$. The cartoons above and below the plots indicate the involvement of the different coherent ensemble states in the four-level system in the PE formation at different magnetic field strengths. The red and blue arrows indicate the optical transitions addressed by excitation with the second pulse of certain circular polarization. The red ovals indicate the superposition state of the coherent ensemble resulting from excitation with the first pulse. The PE, as illustrated by the wave arrow, is emitted when the second pulse [polarization $\sigma^+$ (red) or $\sigma^-$ (blue)] can excite the coherent ensemble for which it has to be in the right superposition state.

Figure 2 shows the calculated magnetic field dependences of the PE amplitude in the circular polarization basis. Initially, a coherent ensemble is created by the first $\sigma^+$ pulse, exciting a coherent superposition of the states ($|+1/2\rangle$, $|+3/2\rangle$). Due to the electron spin precession, the low-energy component of the superposition oscillates between the $|+1/2\rangle$ and $|-1/2\rangle$ ground states at the electron Larmor frequency $\omega_e$. Similarly, the high-energy component oscillates between the $|+3/2\rangle$ and $|-3/2\rangle$ excited states at the effective hole Larmor frequency $\omega_h$. Various states of the coherent ensemble upon arrival of the second pulse are indicated by the red ovals in the illustrations of Fig. 2. Eventually, the PE is generated when the ensemble is in a state that can be excited by the second pulse: This is possible when either the $\sigma^+$ second pulse (red vertical

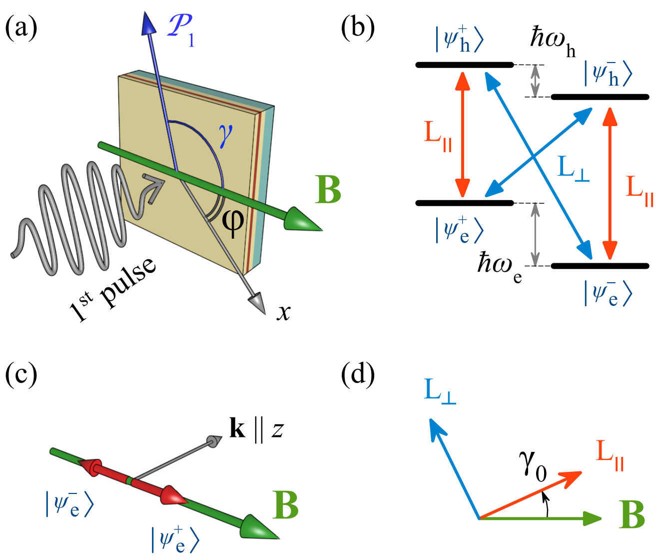


FIG. 3. Experimental geometry and spin level structure in the linear polarization basis. (a) Orientation of the first pulse polarization relative to the magnetic field **B**. (b) Energy level scheme. (c) Electron-spin orientations in the ground states $|\pm 1/2\rangle$, which are split in energy and are not mixed by the magnetic field. (d) Eigenpolarizations $L_{||}$ and $L_\perp$ determined by the angle $\gamma_0$.

arrow) hits the ensemble when it is in the $(|+1/2\rangle, |+3/2\rangle)$ superposition or the $\sigma^-$ second pulse (blue vertical arrow) hits the ensemble in the $(|-1/2\rangle, |-3/2\rangle)$ superposition. As a result, the PE amplitude exhibits two types of oscillations when the magnetic field strength is varied. Typically $|g_e| > |\tilde{g}_h|$; therefore, the fast oscillations are due to the electron spin precession, while the slow oscillations of the envelope are due to the hole spin precession. We note that the signals carry only information about the absolute values of the effective electron and hole in-plane $g$ factors, $|g_e|$ and $|\tilde{g}_h|$, but are insensitive to the relative phase of the electron and hole spin precession.

### B. Linear polarization basis

In case of linearly polarized excitation, the first pulse polarization ($\mathcal{P}_1$) is characterized by the angle $\gamma$ relative to the magnetic field **B**, as shown in Fig. 3(a).

Here, to understand the coherent dynamics of the system, it is convenient to switch to the linear polarization basis shown in Fig. 3(b). It involves as basis states $|\psi_e^\pm\rangle$ and $|\psi_h^\pm\rangle$ with spin projections parallel and antiparallel to the effective magnetic field axis, respectively, and the two linear eigenpolarizations of the system, $L_{||}$ and $L_\perp$. The ground states $|\psi_e^\pm\rangle$ correspond to the two electron spin orientations along the **B** axis, as illustrated in Fig. 3(c), with an energy splitting $\hbar\omega_e$. The excited states $|\psi_h^\pm\rangle$ with an energy splitting $\hbar\omega_h$ have spin orientations along the effective magnetic field that is directed at the angle $\varphi_h$ relative to the $x$ axis. The wave functions of these basis states are

$$\psi_e^\pm = \frac{1}{\sqrt{2}}(e^{-i\varphi_e/2}|+1/2\rangle \pm e^{i\varphi_e/2}|-1/2\rangle),$$

$$\psi_h^\pm = \frac{1}{\sqrt{2}}(e^{-i\varphi_h/2}|+3/2\rangle \pm e^{i\varphi_h/2}|-3/2\rangle) \qquad (5)$$

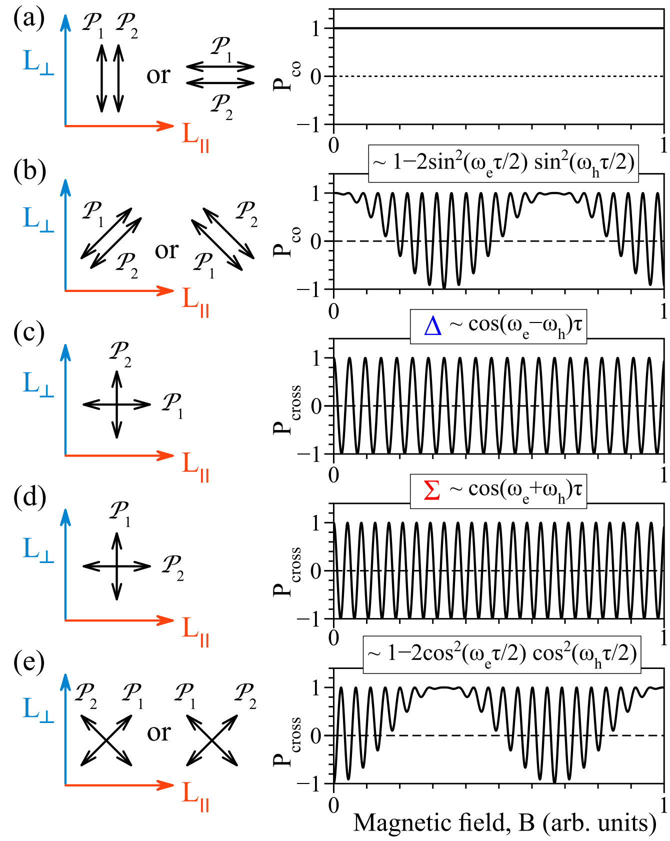


FIG. 4. Magnetic field dependences of the PE amplitude calculated using Eqs. (6), assuming $g_e = 15|\tilde{g}_h|$, for various linear polarization configurations in the eigenpolarization basis $L_{||}, L_\perp$ for a fixed delay $\tau$. (a, b) Co-polarized configurations. (c–e) Cross-polarized configurations. The symbols $\Delta$ and $\Sigma$ denote the PE signals oscillating at the difference and sum Larmor frequencies of the electron and hole, respectively. The black arrows indicate the directions of linear polarization for the first and second pulses.

with $|\pm 1/2\rangle$ and $|\pm 3/2\rangle$ being the circular basis states along the $z$ axis as used before.

The orientation of the eigenpolarization $L_{||}$ is determined by the eigenangle $\gamma_0 = (\varphi_h - \varphi_e)/2 - \varphi + m\pi$, where $m$ is an integer, as depicted in Fig. 3(d) (see Appendix A 3).

Now we analyze the PE in the polarization of the first pulse ($\mathcal{P}_{PE} = \mathcal{P}_1$). The PE amplitudes evaluated for the co- and cross-polarized configurations in Appendix A 4 are given by

$$\begin{aligned} P_{co} &\propto 1 - 2\sin^2(2\alpha)\sin^2(\omega_e\tau/2)\sin^2(\omega_h\tau/2), \\ P_{cross} &\propto \cos[(\omega_e + \omega_h)\tau]\sin^2(\alpha) \\ &\quad + \cos[(\omega_e - \omega_h)\tau]\cos^2(\alpha) \\ &\quad - 2\sin^2(2\alpha)\sin^2(\omega_e\tau/2)\sin^2(\omega_h\tau/2), \end{aligned} \qquad (6)$$

where $\alpha = \gamma - \gamma_0$. We note that the PE detected in polarizations different from that of $\mathcal{P}_1$ contains higher harmonics so that it is harder to extract information from it.

Figure 4 summarizes the magnetic field dependences of the PE amplitude for the main co- and cross-polarized configurations with respect to the eigenpolarization basis $L_{||}, L_\perp$,

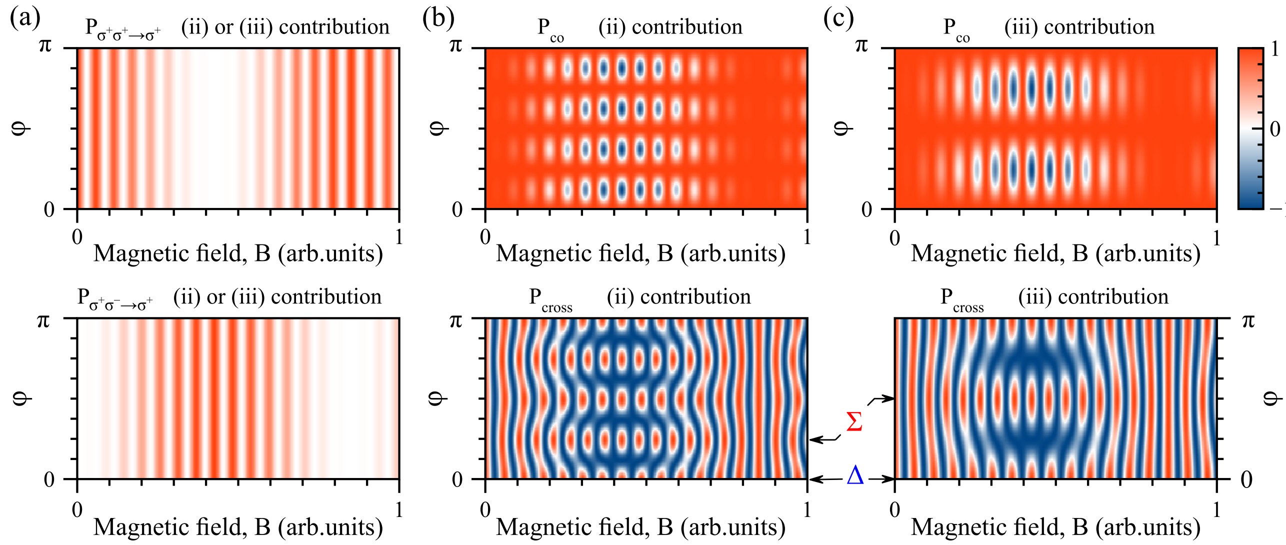


FIG. 5. Spin-dependent PE as a function of the magnetic field strength $B$ and orientation $\varphi$ calculated for different polarization configurations and contributions to the effective hole $g$ factor. Again, $g_e = 15|\tilde{g}_h|$ is taken. (a) Contributions (ii) and (iii) in the circularly co-polarized (top) and cross-polarized (bottom) configurations. (b) Contribution (ii) in the linearly co-polarized (top) and cross-polarized (bottom) configurations. (c) Contribution (iii) in the linearly co-polarized (top) and cross-polarized (bottom) configurations. The symbols $\Delta$ and $\Sigma$ denote the PE signals oscillating at the difference and sum Larmor frequencies of the electron and hole, respectively. The PE in the linear polarization configurations (b) and (c) is considered in the eigenpolarization basis, $\gamma = \gamma_0(\varphi = 0)$.

as sketched in the left part of the figure. The PE amplitude is a constant in the co-polarized configurations $L_{||}L_{||} \to L_{||}$ and $L_\perp L_\perp \to L_\perp$, as shown in Fig. 4(a). The PE amplitude oscillates as $\cos(\omega_e - \omega_h)\tau$ at the difference frequency ($\Delta$) and as $\cos(\omega_e + \omega_h)\tau$ at the sum frequency ($\Sigma$) in the cross-polarized configurations $L_{||}L_\perp \to L_{||}$ and $L_\perp L_{||} \to L_\perp$, respectively, as shown in Figs. 4(c) and 4(d). Finally, Figs. 4(b) and 4(e) display the magnetic field dependences when the pulses are diagonally co- and cross-polarized, respectively. Here, the fast oscillations originate from the electron spin precession, while the slow periodic amplitude modulation of these oscillations emerges from the hole spin precession.

### C. Symmetry of different hole $g$ factor contributions

Next we analyze how the various interactions contributing to the in-plane hole $g$ factor manifest in the spin-dependent PE signal when varying the magnetic field angle $\varphi$ in the QW plane. As before, we consider an isotropic electron in-plane $g$ factor, so that $\varphi_e = \varphi$.

When only a single interaction for the hole out of (i)–(iii) is present, the splitting of the heavy-hole states will be isotropic, independent of the magnetic field angle $\varphi$. Therefore, the magnetic field dependences of the PE, measured in the $\sigma^+\sigma^\pm \to \sigma^+$ configurations, will exhibit no difference when $\varphi$ is varied, similar to the PEs shown in Fig. 2. This is illustrated in Fig. 5(a), implying $\omega_h \propto B$.

However, each of the considered interactions has a distinct symmetry, which is reflected in the spin-dependent PE when measured in the linear polarization configurations. The Zeeman interaction (i), providing the $\omega_z \propto B^3$ splitting and entering the in-plane hole $g$ factor with the phase $\varphi_h = 3\varphi$, results in $\alpha = \gamma$. Thus, the magnetic field dependences of the PE measured with linearly polarized pulses will be independent of the angle $\varphi$, and therefore the contribution (i) is isotropic. The contribution (ii) due to the cubic crystal symmetry with strength $\omega_q$ and phase $\varphi_h = -\varphi$ gives $\alpha = \gamma + 2\varphi$. As a result, the spin-dependent PE measured in the co-polarized configurations contains the eighth harmonic, while the PE measured in the cross-polarized configurations contains the fourth and eighth harmonics when varying the angle $\varphi$, as shown in Fig. 5(b). Finally, the strain-induced interaction (iii) with strength $\omega_{ht}$, which enters the in-plane hole $g$ factor with phase $\varphi_h = \varphi + 2\phi + \pi/2$, leads to $\alpha = \gamma + \varphi + \phi - \pi/4$. This contribution provides the fourth harmonics in the linearly co-polarized configurations, and the second and fourth harmonics in the linearly cross-polarized configurations as function of $\varphi$, as shown in Fig. 5(c).

Superimposing these interactions in accordance with Eq. (2) leads to interference effects, which in general makes the analysis of the experimentally measured spin-dependent PE a nontrivial task. When, however, one of the contributions (i)–(iii) prevails, the spin-dependent PE must exhibit certain symmetry properties, which help to identify the most important contribution and, as a result, simplify the analysis of the data.

## III. EXPERIMENTAL RESULTS

With the aim of studying the hole spin anisotropy by means of spin-dependent PE we used a 20-nm-thick $CdTe/Cd_{0.76}Mg_{0.24}Te$ single QW (no. 032112B). It was grown by molecular-beam epitaxy on a [100]-oriented GaAs substrate overgrown with 4.5-$\mu$m $Cd_{0.76}Mg_{0.24}Te$ buffer and a short-period superlattice. The CdTe QW is sandwiched between 100-nm-thick $Cd_{0.76}Mg_{0.24}Te$ barriers. The QW layer is unintentionally doped by donors ($n_d < 10^{10}$ cm$^{-2}$) leading to the $D^0X$ optical transition at the energy of 1.5973 eV

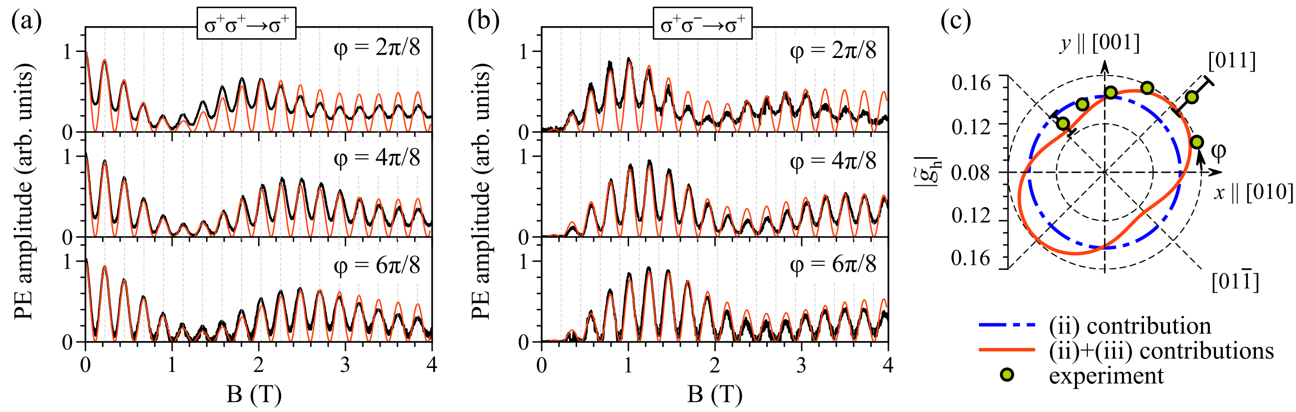


FIG. 6. Summary of the experimental results on the spin-dependent PE measured on $D^0X$ in a CdTe/$Cd_{0.76}Mg_{0.24}$Te QW at $T$=1.5 K for a pulse delay of $\tau = 200$ ps, using circularly polarized pulses. (a, b) Oscillations of the PE amplitude measured at $\varphi = 2\pi/8$, $4\pi/8$, and $6\pi/8$ in the $\sigma^+\sigma^+ \to \sigma^+$ and $\sigma^+\sigma^- \to \sigma^+$ polarization configurations, respectively. The thick black curves are the experimental data; the thin red curves are model calculations, with parameters adjusted to describe the complete data set. (c) Dependence of the absolute value of the effective in-plane hole $g$ factor $|\tilde{g}_h|$ on the in-plane angle $\varphi$ of the magnetic field orientation. The dots are results from the individual data fits; the red solid line gives the contributions (ii) and (iii) from the complete data set modeling; the blue dash-dotted circle gives the contribution (ii) alone.

($T = 1.5$ K), which we excite resonantly (for details see Appendix B 1). The structure was examined before by various photon echo-based techniques and can be considered as a model system for studies that can be performed also on many other structures [19,24–26].

The experimental setup we employ here allows for time-resolved degenerate four-wave mixing (FWM) measurements. The sample was cooled down to the temperature of 1.5 K in a helium bath cryostat, equipped with a superconducting split-coil magnet. Two pulse trains from a Ti:sapphire laser with the spectral width of 0.9 meV (duration 2.3 ps) and wave vectors $\mathbf{k}_1$ and $\mathbf{k}_2$, oriented close to the sample normal, were focused into a spot of about 250 $\mu$m on the sample. The second pulse train was delayed with an optical delay line by $\tau = 200$ ps relative to the first one. The PE signal was collected in the reflection geometry along the $2\mathbf{k}_2 - \mathbf{k}_1$ direction and mixed at the photodetector with a reference pulse, delayed by $2\tau = 400$ ps with respect to the first pulse. The desired polarization of the detected FWM signal was chosen by the reference pulse polarization. The detected signal intensity is $I \propto E_{\rm PE}E_{\rm Ref}$, where $E_{\rm PE}$ and $E_{\rm Ref}$ are the electric-field amplitudes of the PE and reference pulse, respectively. The energies per pulse were about 10 pJ, which corresponds to the pulse area of about $\pi/2$ or less [25]. More details on the implemented technique can be found in Ref. [27]. The transverse magnetic field was applied in the sample plane at various angles $\varphi = n\pi/8$, $n = 1$–6. The magnetic field strength was scanned in the range $B = 0$–4 T.

Figures 6(a) and 6(b) display PE measurements, performed in the $\sigma^+\sigma^+ \to \sigma^+$ or $\sigma^+\sigma^- \to \sigma^+$ polarization configurations, for $\varphi = 2\pi/8, 4\pi/8$, and $6\pi/8$. The data for the full set of $\varphi$ angles is presented in Appendix B 2. These data manifest two types of oscillations in full accord with our theoretical considerations [see Eq. (4) and Fig. 2]. The fast oscillations follow a frequency independent of the angle $\varphi$. From these oscillations the electron $g$ factor $|g_e| = 1.584 \pm 0.005$ is extracted, in good agreement with previous studies [26,28]. The envelope function of the fast oscillations exhibits slow oscillations caused by the hole spin precession. These slow oscillations appear to be in antiphase for the $\sigma^+\sigma^+ \to \sigma^+$ and $\sigma^+\sigma^- \to \sigma^+$ polarization configurations and demonstrate a $\varphi$-dependent period. From that period the effective in-plane hole $g$ factor $|\tilde{g}_h| = \hbar\omega_h/\mu_B B$ can be determined, as plotted with dots in Fig. 6(c). It varies in the range $|\tilde{g}_h|$=0.13–0.17 with the highest value for the magnetic field oriented along the [011] crystalline axis.

Figure 7 provides experimental data measured in the linear polarization configurations for the magnetic field orientations $\varphi = 3\pi/8, 4\pi/8$, and $5\pi/8$. Further experimental data can be found in Appendix B 3. In order to operate with specific linear polarizations in the laboratory reference frame associated with the magnetic field orientation we employ the following directions, as indicated in the inset of Fig. 7: horizontal H||**B** ($\gamma = 0$), vertical V $\perp$ **B** ($\gamma = \pi/2$), diagonal D ($\gamma = \pi/4$), and antidiagonal A $\perp$ D ($\gamma = 3\pi/4$). The data exhibit the following symmetry properties: In the co-polarized configurations HH $\to$ H and DD $\to$ D, the signal shape changes with the angle $\varphi$ with an oscillation period of $\pi/4$, corresponding to the eighth harmonic. Similarly, in the cross-polarized configurations HV $\to$ H (VH $\to$ V) and DA $\to$ D (AD $\to$ A) periodic shape changes occur with the angle period of $\pi/2$, which corresponds to the fourth harmonic. However, the anisotropic angular dependence of the effective hole $g$ factor [Fig. 6(c)] evidences the presence of at least two different contributions, one of which is thus prevailing.

## IV. ANALYSIS AND DISCUSSION

From the comparison of the data in Fig. 7 with the magnetic field dependences of the PE in the eigenpolarization basis (Fig. 4), the orientation of this basis can be deduced: $\gamma_0 \approx -2\varphi + m\pi$. We note that the measured signal is proportional to the absolute value of the PE amplitude, so that it should be compared with the $|P_{\rm co}|$ and $|P_{\rm cross}|$ dependences. As a result, for the magnetic field tilted by $\varphi = 3\pi/8$ the eigenangle is $\gamma_0 \approx \pi/4$. Thus, the eigenpolarizations $L_{||}$ and $L_\perp$ are aligned with the D and A polarizations, respectively, as shown schematically in Fig. 7(a). Similarly, the data measured at $\varphi = 4\pi/8$ [Fig. 7(b)] have the eigenangle $\gamma_0 \approx 0$ and the

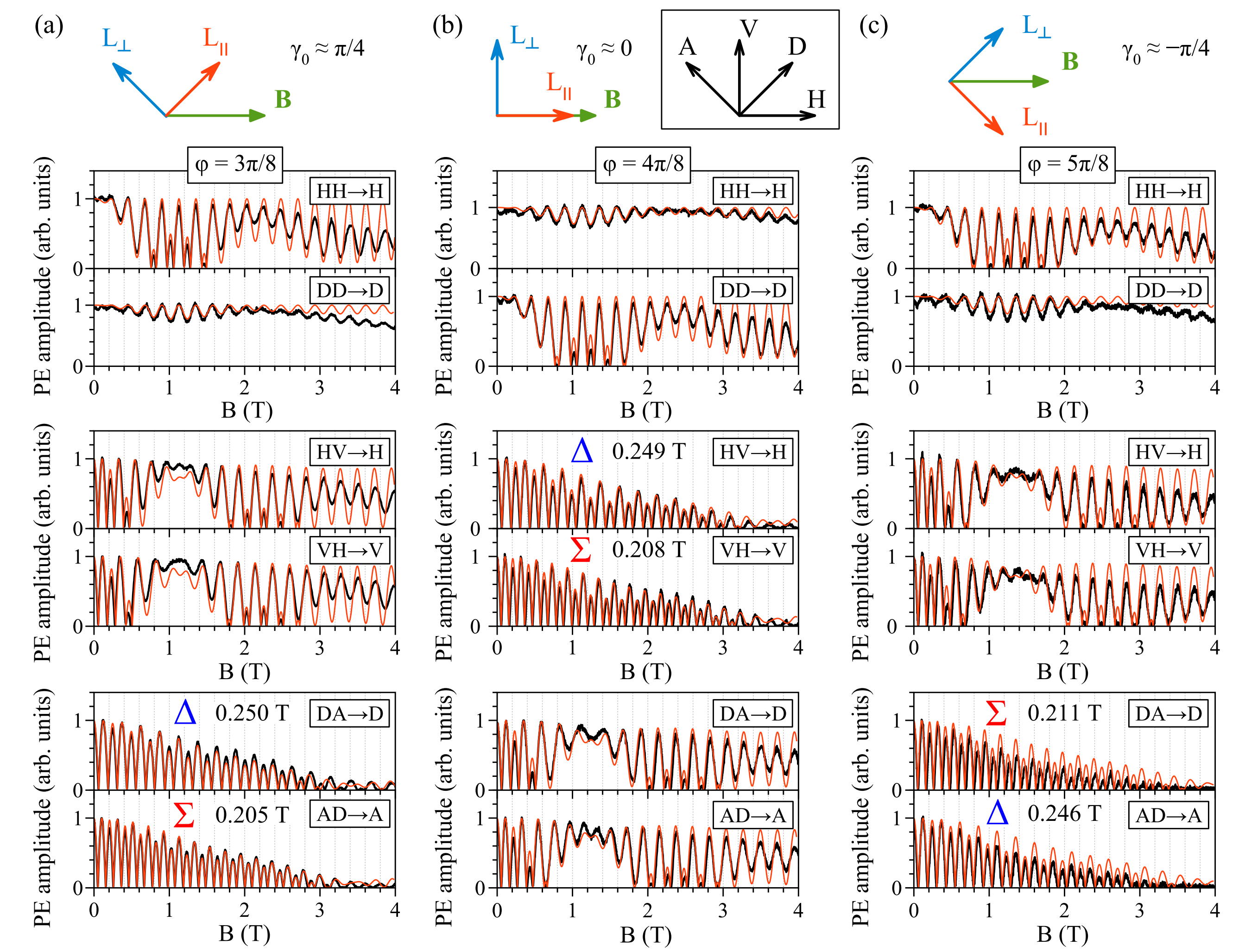


FIG. 7. Spin-dependent PE measured with linearly polarized pulses at $\tau = 200$ ps in various polarization configurations for different magnetic field orientation angles: (a) $\varphi = 3\pi/8$, (b) $\varphi = 4\pi/8$, and (c) $\varphi = 5\pi/8$. The experimental data (thick black curves) are normalized to unity. The thin red curves correspond to model calculations with parameters chosen to describe the complete data set. The schemes above the data depict the orientations of the eigenpolarizations $L_{||}$ and $L_\perp$. The arrows in the box give the linear polarization directions in the laboratory reference frame: H, D, V, and A correspond to the angles zero, $\pi/4$, $\pi/2$, and $3\pi/4$ with respect to the **B** axis. The numbers next to the $\Delta$ and $\Sigma$ symbols give the extracted difference and sum oscillation periods.

$L_{||}, L_\perp$ axes are aligned with the H and V polarizations. Accordingly, the data measured at $\varphi = 5\pi/8$ [Fig. 7(c)] have the eigenangle $\gamma_0 \approx -\pi/4$ and the $L_{||}, L_\perp$ axes are aligned with the A and D polarizations.

We discuss now the details of the model adjusted to describe quantitatively the whole collection of experimental data. First, we neglect the Zeeman contribution (i) to the hole $g$ factor, since it is expected to be small ($\omega_z \sim \omega_h \times 10^{-3}$) due to the sufficiently large HH-LH splitting of $\Delta_{\mathrm{LH}} \approx 15$ meV [24]. Moreover, it requires a nonlinear dependence of the Zeeman splitting on the magnetic field, which is hard to resolve from our data. In order to take into account the inhomogeneity of the hole $g$ factor, we consider Gaussian distributions of the two remaining contributions weights $q$ and $u$ with the same relative dispersions $\Delta p/p$ ($p = q, u$), for simplicity. We neglect the $g_e$ dispersion, which is expected to be within 1% [28,29].

From the theoretical modeling of the complete data set shown with the red lines in Figs. 6(a), 6(b), and 7 we find that the in-plane hole $g$ factor is dominated by the non-Zeeman contribution (ii) with the Luttinger parameter $q = 0.095 \pm 0.005$. It is responsible for the main symmetry properties of the spin-dependent PE and corresponds to the effective hole $g$ factor $3/2q \approx 0.143$, shown in Fig. 6(c) with

TABLE I. The parameter values used to describe the complete set of experimental data shown in Figs. 9 and 10.

| $\tau$ (ps) | $\Delta_{\mathrm{LH}}$ (eV) | $g_e$ | $\Delta g_e$ | $g_h$ | $q$ | $\Delta q/q$ | $u$ | $\Delta u/u$ | $\phi$ (deg) | $\delta\varphi$ (deg) |
|---|---|---|---|---|---|---|---|---|---|---|
| 200 | 0.015 | 1.584 | 0 | 1 | 0.095 | 0.25 | 0.016 | 0.25 | 94 | 4 |

the blue dash-dotted circle. The strain-induced contribution (iii) has the weight of $u = 0.016 \pm 0.006$ with the strain axis orientation $\phi = (94 \pm 2)^\circ$. This contribution interferes with the non-Zeeman contribution (ii) leading to the anisotropic angular dependence of the observed effective in-plane hole $g$ factor, shown in Fig. 6(c) with the red solid line. The dependence is stretched along the [011] axis with the aspect ratio of about 30%, resulting in the hole effective $g$ factor varying in the range $|\tilde{g}_h|$=0.125–0.160.

The small amplitude oscillations observed in the linearly co-polarized configurations aligned with the $L_{||}$ axis, such as HH → H at $\varphi = 4\pi/8$ [Fig. 7(b)] or DD → D at $\varphi = 3\pi/8$ and $5\pi/8$ [Figs. 7(a) and 7(c)], are due to a deviation $\delta\varphi \sim 4^\circ$ of the experimentally used sample orientations from the nominal $\varphi$ angles with respect to the actual crystal $x$ axis. This deviation was confirmed by an x-ray Laue analysis.

Finally, the dispersion of the hole $g$ factor can be characterized by the standard deviation $\Delta p/p \approx 0.25$. It is responsible for the strong damping of the oscillating PE amplitude with increasing magnetic field strength $B$ in the $\Delta$ and $\Sigma$ polarization configurations such as HV → H (VH → V) at $\varphi = 4\pi/8$ or DA → D (AD → A) at $\varphi = 3\pi/8$ and $5\pi/8$ (Fig. 7). It causes also the contrast reduction in the PE amplitude oscillations in the $\sigma^+\sigma^\pm \to \sigma^+$ polarization configurations (Fig. 6).

There are other magnetic-field-induced effects to mention, which we, however, neglected here. Because of the diamagnetic high-energy shift of the $D^0X$ spectral line (≈0.3 meV at $B = 4$ T) and the subsequent detuning from the laser energy, the detected PE amplitude is somewhat reduced at $B > 2$ T. Additionally, the strong magnetic field affects the spin dynamics during the optical pulse action, which may effectively reduce the detected PE amplitude. As was mentioned before, the pulse delay $\tau$ can be varied at constant magnetic field in order to observe the spin-dependent PE. Thereby, the diamagnetic shift problem can be eliminated. However, since the PE amplitude shows an exponential decay with the optical coherence time ($T_2 \approx 100$ ps) (see Appendix B1 and Ref. [25]), this has to be taken into account. The spin-relaxation processes occur during much longer times ($\geqslant 1$ ns) and can still be neglected [26].

Previous studies of the in-plane hole spin anisotropy were mainly based on the angular dependence of linear polarization for the photoluminescence of exciton complexes subject to a transverse external magnetic field. The spin anisotropy was studied in diluted magnetic II-VI semiconductor QWs [4,9] and nonmagnetic self-assembled QDs based on II-VI and III-V compounds [5,6,22,23]. In diluted magnetic CdTe/(Cd,Mn)Te [4] and (Cd,Mn)Te/(Cd,Mn,Mg)Te QWs [9] all main mechanisms (i)–(iii) were evaluated in detail. Diluted magnetic semiconductors possess a giant Zeeman splitting due to the exchange interaction with the $Mn^{2+}$ ions and therefore the isotropic contribution (i) is relevant in moderate magnetic fields of several Tesla. In addition, it was demonstrated that the lowering to $C_{2v}$ crystal symmetry due to strain or shape anisotropy leads to the dominating role of the term (iii), while the cubic anisotropy (ii) is weak. The in-plane hole spin anisotropy in nonmagnetic structures was investigated only for self-assembled QDs. In this case the Zeeman contribution (i) is negligible due to the large splitting of the heavy- and light-hole states given by the confinement along the growth direction. Here, the strong influence of term (iii) due to strain and shape anisotropy was demonstrated for single CdSe/ZnSe and (In,Ga)As/GaAs QDs [5,23]. Subsequent studies demonstrated also the importance of the cubic anisotropy in some QDs where term (iii) is reduced to values comparable with term (ii) [6,22]. However, no evaluation of the $q$ parameter was possible in previous studies. Surprisingly, in our paper we observe that the cubic crystal symmetry plays the dominant role in the anisotropic hole spin properties of nonmagnetic CdTe/(Cd,Mg)Te QW structures. Thereby, we can determine the Luttinger parameter, which in quantum wells was not studied in detail experimentally so far. It is usually disregarded because of its hypothetical smallness [30–32]. For GaAs-based QWs, values in the range $q = 0.01$–$0.04$ were evaluated from photoluminescence studies [21,33]. The magnitude of $q = 0.095 \pm 0.005$ evaluated with high precision in our paper is noticeably larger.

## V. CONCLUSIONS

A photon echo-based technique has been developed to monitor the precise spin-dependent coherent optical response of ensembles of exciton complexes subject to a transverse external magnetic field with arbitrary direction within the sample plane. It may be applied to study charged excitons as well as neutral excitons bound to a donor or an acceptor in various semiconductor systems including quantum wells, quantum dot ensembles, and epilayers, which can be well described by a four-level energy scheme with Kramers doublets in the ground and excited states. We demonstrate that the photon echo resulting from a sequence of two circularly polarized pulses carries only information about the absolute values of the effective electron and hole in-plane $g$ factors and is not sensitive to the relative phase of the electron and hole spin precession. Excitation by linearly polarized pulses gives rich information not only on the Zeeman splitting of electronic states. It allows one also to determine precisely the eigenpolarizations of the optical transitions which depend on the relative orientation of the magnetic field and sample. We show that the angular dependences of the photon echo signal contain different harmonics which can be uniquely attributed to the mechanisms responsible for the magnetic anisotropy such as crystal symmetry, strain, or shape anisotropy.

The main advantage of the technique is the possibility to measure the in-plane components of the hole $g$ factor using relatively weak magnetic fields in inhomogeneously broadened ensembles and to study various interactions of the hole spin with the in-plane magnetic field. In our paper, a magnetic field as low as $B \approx 200$ mT was sufficient to estimate the effective hole $g$ factor of about 0.1 from spin-dependent photon echo measurements in certain polarization configurations at the pulse delay $\tau = 200$ ps. This is because the effective hole $g$ factor can be evaluated from the deviation of the signal oscillation frequency from the electron Larmor frequency. Also, the magnetic field strength can be scaled down further with increasing $\tau$. Moreover, as compared with other methods studying the hole spin dynamics, it is not necessary to have resident holes for that purpose. Eventually, applying the method to a CdTe/(Cd,Mg)Te quantum well we have been able to extract the parameter $q$ in the Luttinger-Kohn Hamiltonian, which is difficult to obtain by other optical techniques. The presented method can be extended for magnetic fields tilted from the structure plane, allowing thus for studying the out-of-plane hole spin properties.

## ACKNOWLEDGMENTS

The authors are thankful to Yu. G. Kusrayev, A. V. Trifonov, and M. M. Glazov for fruitful discussions. The authors acknowledge financial support by the Deutsche Forschungsgemeinschaft through the International Collaborative Research Centre Transregio 160 (Projects No. A3 and No. A1). S.V.P. and I.A.Y. thank the Russian Foundation for Basic Research (Project No. 19-52-12046) and the Saint Petersburg State University (Grant No. 51125686). The research in Poland was partially supported by the Foundation for Polish Science through the International Research Agendas Programme, co-financed by the European Union within Smart Growth Operational Programme and by the National Science Centre through Grants No. 2017/25/B/ST3/02966 and No. 2018/30/M/ST3/00276.

## APPENDIX A: THEORETICAL DESCRIPTION OF MAGNETIC-FIELD-DEPENDENT PHOTON ECHOES

In order to describe the optical excitation of the negatively charged trion by a short laser pulse with central frequency $\omega$ close to the trion resonance frequency $\omega_0$ and the resulting dynamics in a magnetic field we use a $4 \times 4$ time-dependent density matrix, comprising the two electron spin projections $(\pm 1/2)$ (index 1 and 2) and the two hole spin projections $(\pm 3/2)$ (index 3 and 4).

The temporal evolution of the density matrix is described by the Lindblad equation:

$$\dot{\rho} = -\frac{i}{\hbar}[\hat{H}, \rho] + \Gamma. \tag{A1}$$

Here $\hat{H}$ is the Hamiltonian of the system and $\Gamma$ describes relaxation processes phenomenologically. In our case the Hamiltonian contains three contributions: $\hat{H} = \hat{H}_0 + \hat{H}_B + \hat{V}$, where $\hat{H}_0$ is the Hamiltonian of the unperturbed spin system, $\hat{H}_B$ gives the interaction with the magnetic field, and $\hat{V}$ describes the interaction with the light pulses. In the calculations we use the short pulse approximation assuming that the pulse duration is significantly shorter than the trion lifetime, the decoherence times, and the electron spin precession period in the transverse magnetic field. This assumption is justified for our experimental conditions.

### 1. Electron-trion system under the action of a short light pulse

The interaction with the electromagnetic wave in the electric-dipole approximation is described by the Hamiltonian:

$$\hat{V}(t) = -\int [\hat{d}_+(\boldsymbol{r})E_{\sigma^+}(\boldsymbol{r}, t) + \hat{d}_-(\boldsymbol{r})E_{\sigma^-}(\boldsymbol{r}, t)]d^3r, \tag{A2}$$

where $\hat{d}_\pm(\boldsymbol{r})$ are the circularly polarized components of the dipole moment density operator, and $E_{\sigma^\pm}(\boldsymbol{r}, t)$ are the correspondingly polarized components of the electric field of a quasimonochromatic electromagnetic wave. The electric field of this wave is given by

$$\boldsymbol{E}(\boldsymbol{r}, t) = E_{\sigma^+}(\boldsymbol{r}, t)\boldsymbol{o}_+ + E_{\sigma^-}(\boldsymbol{r}, t)\boldsymbol{o}_- + \text{c.c.}, \tag{A3}$$

where $\boldsymbol{o}_\pm$ are the circularly polarized unit vectors that are related to the unit vectors $\boldsymbol{o}_x \parallel x$ and $\boldsymbol{o}_y \parallel y$ through $\boldsymbol{o}_\pm = (\boldsymbol{o}_x \pm i\boldsymbol{o}_y)/\sqrt{2}$. Here the components $E_{\sigma^+}$ and $E_{\sigma^-}$ contain the temporal phase factors $e^{-i\omega t}$.

The strength of the light interaction with the electron-trion system is characterized by the corresponding transition matrix element of the operators $\hat{d}_\pm(\boldsymbol{r})$ calculated with the wave functions of the valence band, $|\pm 3/2\rangle$, and the conduction band, $|\pm 1/2\rangle$ [34]:

$$d(\boldsymbol{r}) = \langle +1/2|\hat{d}_-(\boldsymbol{r})| + 3/2\rangle = \langle -1/2|\hat{d}_+(\boldsymbol{r})| - 3/2\rangle. \tag{A4}$$

The Hamiltonian $\hat{H} = \hat{H}_0 + \hat{V}$ in our basis is given by

$$H_0 + V = \frac{\hbar}{2}\begin{pmatrix} 0 & 0 & f_+^* e^{i\omega t} & 0 \\ 0 & 0 & 0 & f_-^* e^{i\omega t} \\ f_+ e^{-i\omega t} & 0 & 2\omega_0 & 0 \\ 0 & f_- e^{-i\omega t} & 0 & 2\omega_0 \end{pmatrix}. \tag{A5}$$

The $f_\pm(t)$ are proportional to the smooth envelopes of the circularly polarized components $\sigma^+$ and $\sigma^-$ of the excitation pulse, given by

$$f_\pm(t) = -\frac{2e^{i\omega t \mp i(\gamma+\varphi)}}{\hbar}\int d(\boldsymbol{r})E_{\sigma_\pm}(\boldsymbol{r}, t)d^3r.$$

Here $(\gamma + \varphi)$ is the angle between the $x$ axis and the polarization plane of light if it is linearly polarized. For simplicity we consider pulses with rectangular shape [35].

### 2. Precession in the magnetic field

Next, we consider the magnetic field effect. The magnetic field **B** is applied perpendicular to the propagation direction of the incident light at an angle $\varphi$ relative to the $x$ axis. The

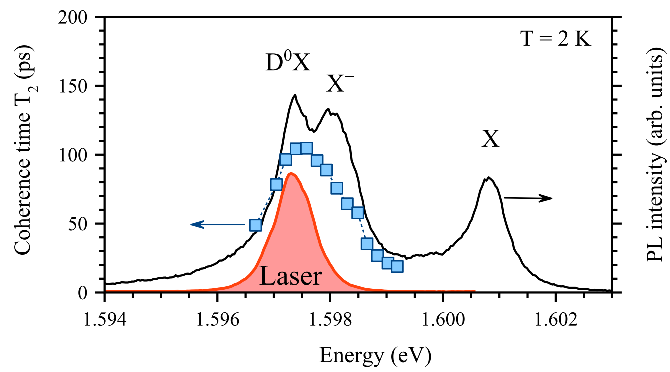


FIG. 8. PL spectrum of the studied 20-nm-thick $CdTe/Cd_{0.76}Mg_{0.24}Te$ single QW (black line) and spectral dependence of the optical coherence time $T_2$ (blue squares) measured at the temperature of 2 K (from Ref. [25]). $D^0X$ denotes the donor-bound exciton; $X^-$ and X denote the negatively charged and neutral exciton, respectively. The red shaded area indicates the laser pulse spectrum at the energy of 1.5973 eV.

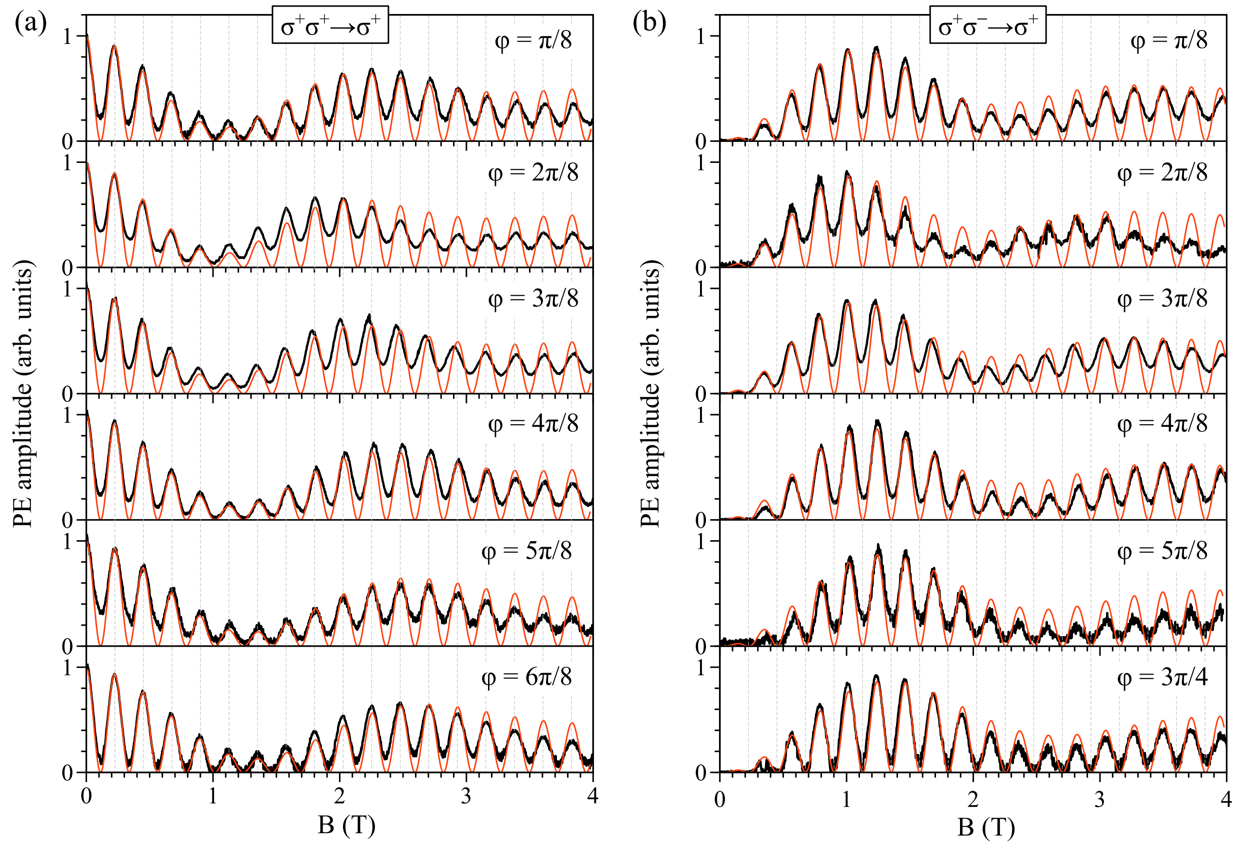


FIG. 9. Magnetic field dependences of the PE amplitude measured in circularly (a) co-polarized and (b) cross-polarized configuration at magnetic field angles $\varphi = n\pi/8, n = 1..6$. The delay time between the optical pulses is $\tau = 200$ ps. The data are shown with the black line. The red line corresponds to the theoretical simulation of the data using the model parameters given in Table I. The periodic vertical grid is drawn with a step according to the spacing between the oscillation maxima in the $\sigma^+\sigma^+ \to \sigma^+$ configuration.

corresponding Hamiltonian is

$$H_B = \frac{\hbar}{2}\begin{pmatrix} 0 & \omega_e e^{-i\varphi_e} & 0 & 0 \\ \omega_e e^{i\varphi_e} & 0 & 0 & 0 \\ 0 & 0 & 0 & \omega_h e^{-i\varphi_h} \\ 0 & 0 & \omega_h e^{i\varphi_h} & 0 \end{pmatrix}, \tag{A6}$$

where $\omega_{e,h}$ and $\varphi_{e,h}$ are the electron and hole (trion) precession frequencies and the angles between the $x$ axis and the effective magnetic field axes, respectively. The angles $\varphi_{e,h}$ differ from the angle $\varphi$ because of possible anisotropies of the electron and hole $g$ factors. For the electron in the ground state, we assume the in-plane $g$ factor $g_e$ to be isotropic. The Larmor frequency of the electron is $\omega_e = g_e\mu_B B/\hbar$, where $\mu_B$ is the Bohr magneton. $\varphi_e = \varphi$.

The hole $g$ factor is known to be strongly anisotropic in the QW plane [4]. Following the theoretical approach by Semenov and Ryabchenko [3] we consider three contributions to the Hamiltonian of the heavy hole in a magnetic field:

$$\omega_h e^{i\varphi_h} = \omega_z e^{3i\varphi} + \omega_q e^{-i\varphi} + \omega_{ht} e^{i(\varphi+2\phi+\pi/2)}. \tag{A7}$$

### 3. Linear basis

For linearly polarized optical excitation it is convenient to diagonalize the Hamiltonian using as a basis the magnetic field eigenstates, so that the field appears only on the diagonal. These spin states for the electron $\Psi_e^{\pm}$ and hole $\Psi_h^{\pm}$ are given by

$$\psi_e^{\pm} = \frac{1}{\sqrt{2}}(e^{-i\varphi_e/2}|+1/2\rangle \pm e^{i\varphi_e/2}|-1/2\rangle),$$
$$\psi_h^{\pm} = \frac{1}{\sqrt{2}}(e^{-i\varphi_h/2}|+3/2\rangle \pm e^{i\varphi_h/2}|-3/2\rangle). \tag{A8}$$

Then one can rewrite the Hamiltonian in this basis:

$$H = \frac{\hbar}{2}\begin{pmatrix} \omega_e & 0 & V_{||}^* e^{i\omega t} & V_{\perp}^* e^{i\omega t} \\ 0 & -\omega_e & V_{\perp}^* e^{i\omega t} & V_{||}^* e^{i\omega t} \\ V_{||}e^{-i\omega t} & V_{\perp}e^{-i\omega t} & 2\omega_0 + \omega_h & 0 \\ V_{\perp}e^{-i\omega t} & V_{||}e^{-i\omega t} & 0 & 2\omega_0 - \omega_h \end{pmatrix}. \tag{A9}$$

Here $V_{||}$ and $V_{\perp}$ are

$$V_{||} = \frac{\hbar}{4}(f_+ e^{-i(\gamma-\gamma_0)} + f_- e^{i(\gamma-\gamma_0)}),$$
$$V_{\perp} = \frac{\hbar}{4}(f_+ e^{-i(\gamma-\gamma_0)} - f_- e^{i(\gamma-\gamma_0)}),$$
$$\gamma_0 = (\varphi_h - \varphi_e)/2 - \varphi + m\pi. \tag{A10}$$

### 4. Photon echo amplitude

Using the procedure described in Ref. [18] one can write the PE amplitude for excitation by two linearly polarized

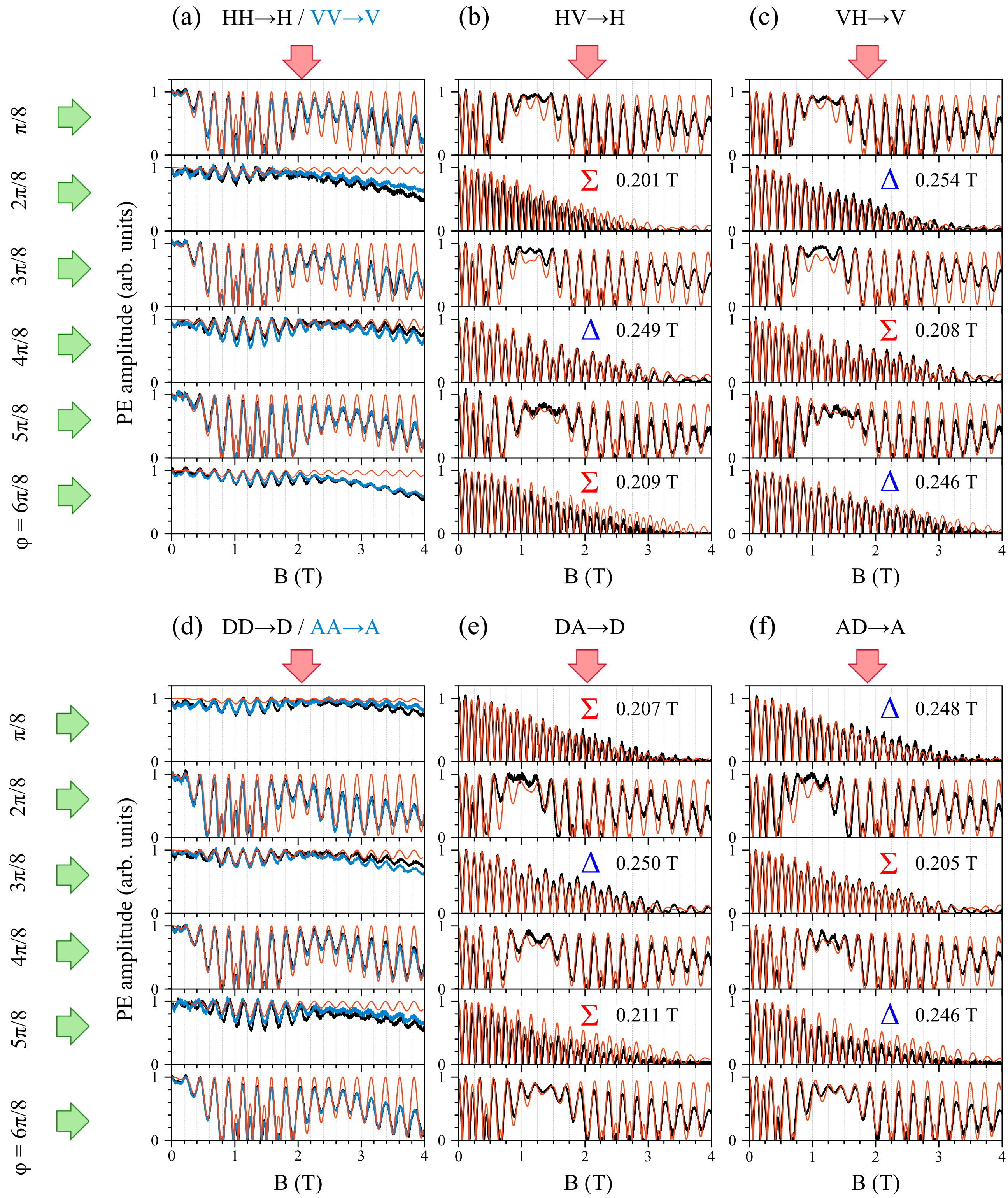


FIG. 10. Magnetic field dependences of the PE amplitude measured in the (a) HH → H/VV → V, (b) HV → H, (c) VH → V, (d) DD → D/AA → A, (e) DA → D, and (f) AD → A linear polarization configurations for the magnetic field angles $\varphi = n\pi/8$, $n = 1$–6. The delay time between the optical pulses is $\tau = 200$ ps. The data are shown with the black (HH → H, HV → H, VH → V, DD → D, DA → D, AD → A) and blue (VV → V, AA → A) lines. The red line corresponds to the data simulation using the model parameters given in Table I. The symbols Δ and Σ indicate the signals oscillating at the difference and sum of Larmor frequencies of the electron and hole, respectively. The numbers next to the Δ and Σ symbols indicate the oscillation periods.

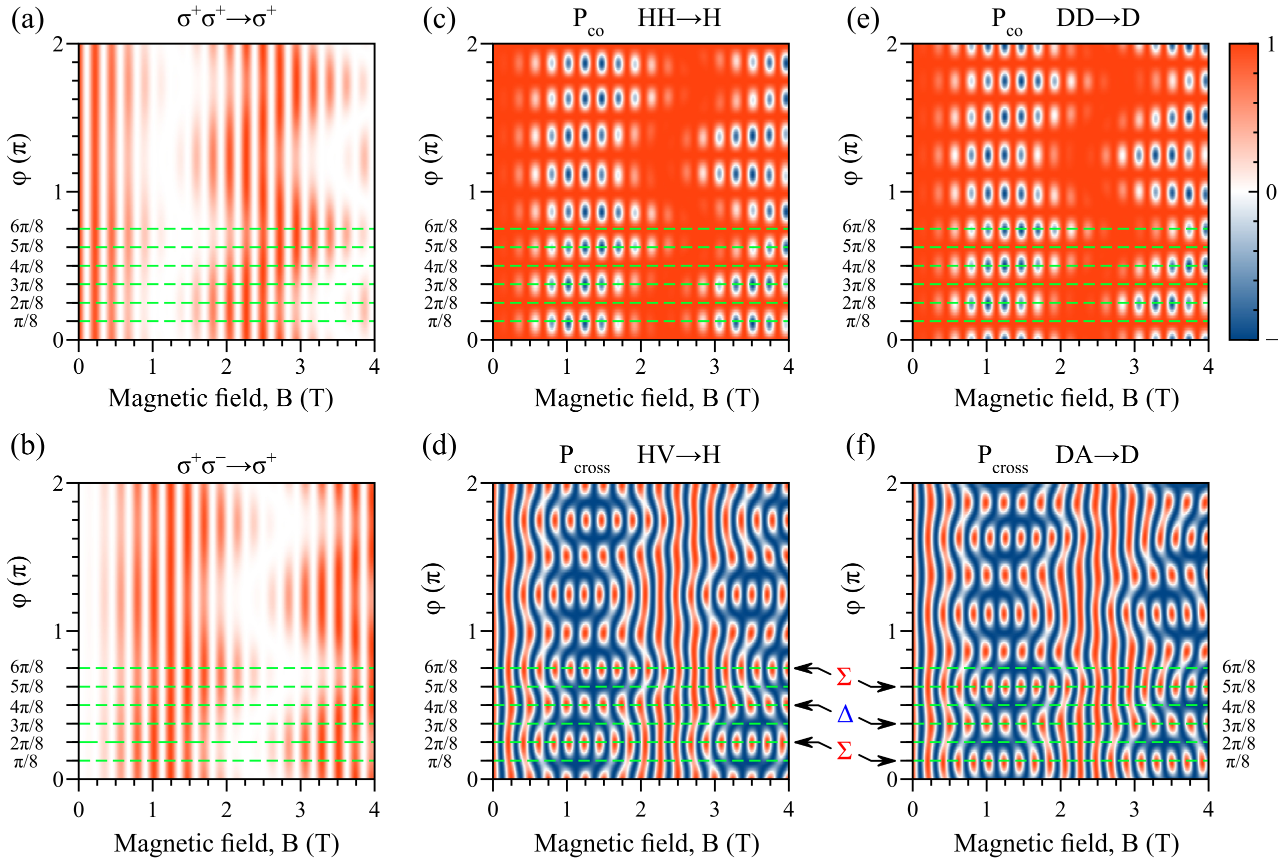


FIG. 11. Simulated variations of the magnetic field dependence of the PE amplitude with the in-plane magnetic field angle $\varphi$ at $\gamma = 0$ and the in-plane hole $g$ factor dispersion ($\Delta g_h = 0$) set to zero in the following polarization configurations: (a, b) circular polarizations $\sigma^+\sigma^\pm \to \sigma^+$, (c, d) linear polarizations HH(V) $\to$ H, and (e, f) linear polarizations DD(A) $\to$ D. The green dashed lines indicate the angles $\varphi$, at which the experimental data were measured. Here, zero hole $g$ factor dispersions ($\Delta q = 0$, $\Delta u = 0$) were used in the simulation in combination with the other parameter values given in Table I.

pulses (angles $\gamma_1$ and $\gamma_2$ relative to the magnetic field direction) and PE analysis with linear polarization (angle $\gamma_3$) as

$$\begin{aligned} P \sim\; & [\sin(\omega_e\tau)\sin(\omega_h\tau)\cos(2\gamma_2 - 2\gamma_0) \\ & + 1 - \cos(\omega_e\tau)\cos(\omega_h\tau)]\cos(\gamma_3 - \gamma_1) \\ & + [(1 + \cos(\omega_e\tau)\cos(\omega_h\tau))\cos(2\gamma_2 - 2\gamma_0) \\ & - \sin(\omega_e\tau)\sin(\omega_h\tau)]\cos(\gamma_3 + \gamma_1 - 2\gamma_0) \\ & + [\cos(\omega_e\tau) + \cos(\omega_h\tau)] \\ & \times \sin(2\gamma_2 - 2\gamma_0)\sin(\gamma_3 + \gamma_1 - 2\gamma_0). \end{aligned} \tag{A11}$$

For co-polarized excitation and detection ($\gamma_1 = \gamma_2 = \gamma_3 = \gamma$) $P$ is given by

$$P_{\rm co} \sim 1 - 2\sin^2(2\alpha)\sin(\omega_e\tau/2)\sin(\omega_h\tau/2), \tag{A12}$$

where $\alpha = \gamma - \gamma_0$.

For cross-polarized excitation ($\gamma_2 = \gamma_1 + \pi/2$) and analysis with $\gamma_3 = \gamma_1 = \gamma$ the PE amplitude is proportional to

$$\begin{aligned} P_{\rm cross} \sim\; & \{\cos[(\omega_e + \omega_h)\tau]\sin^2(\alpha) \\ & + \cos[(\omega_e - \omega_h)\tau]\cos^2(\alpha)\} \\ & - 2\sin^2(2\alpha)\sin(\omega_e\tau/2)\sin(\omega_h\tau/2). \end{aligned} \tag{A13}$$

## APPENDIX B: ADDITIONAL EXPERIMENTAL DATA

### 1. Photoluminescence and optical coherence time spectra

The photoluminescence (PL) of the studied structure measured at temperature $T = 2$ K is shown in Fig. 8. It manifests three features associated with the donor-bound exciton ($D^0X$), the neutral exciton ($X$), and the negatively charged exciton (trion, $X^-$). Although the $D^0X$ and $X^-$ transitions have a similar energy-level structure, as pointed out in the main text, only the donor-bound exciton is studied in detail.

The spectral dependence of the optical coherence time $T_2$ measured earlier in Ref. [25] through the PE decay for varying pulse delay $\tau$ is shown in Fig. 8 by the blue squares. It manifests a maximum value of about 100 ps around the $D^0X$ transition, which allows detection of the PE signal with a high signal-to-noise ratio at delays of $\tau \geqslant 200$ ps.

### 2. Spin-dependent photon echoes in circular polarizations

Here we present the complete set of experimental data on the spin-dependent PE measured on the studied single CdTe/(Cd,Mg)Te QW.

Figure 9 summarizes the magnetic field dependences of the PE amplitude measured in the $\sigma^+\sigma^\pm \to \sigma^+$ polarization configurations at six different magnetic field angles $\varphi$ changed in steps of $\pi/8$. As can be seen, the oscillations in the two polarization configurations are in antiphase. The envelope of the fast oscillations does not reach zero in both polarization configurations. According to our model, this is due to the significant spread of the effective hole $g$ factors. This results also in the damping of the second maximum of the slow oscillations. We have confirmed that swapping between the $\sigma^+$ and $\sigma^-$ polarizations allows accurate reproduction of the measurements.

#### 3. Spin-dependent photon echoes in linear polarizations

Figure 10 displays data measured in the linear polarization configurations, applying the same conditions. The measurements carried out in the co-polarized HH → H configuration essentially reproduce the data obtained in the VV → V configuration. Similarly, the data recorded in the DD → D and AA → A polarization configurations basically coincide for a particular $\varphi$ angle. According to the model, indeed, $P_{co}(\gamma) \equiv P_{co}(\gamma + \pi/2)$ regardless of the angle $\varphi$.

The spin-dependent PE measured in the co-polarized configurations HH → H (VV → V) and DD → D (AA → A) clearly exhibits a periodic alternation of the magnetic field dependence between the two signal types shown in Figs. 4(a) and 4(b) of the main paper with changing the angle $\varphi$ in steps of $\pi/4$. The fast oscillations observed for all angles $\varphi$ have the same period and originate purely from the electron Larmor precession.

In the cross-polarized configurations HV → H (VH → V) and DA → D (AD → A) the magnetic field dependence of the PE alternates periodically between the types of oscillation patterns shown in Figs. 4(c)–4(e) of the main paper with the step in angle $\varphi$ being now $\pi/2$.

Figure 11 displays the simulated PE dependence on the in-plane magnetic field $B$ and the magnetic field angle $\varphi$ for various polarization configurations. The dispersions of the $g$ factors were neglected here ($\Delta q = 0$, $\Delta u = 0$).


[1] *Spin Physics in Semiconductors*, edited by M. I. Dyakonov (Springer, New York, 2017).

[2] H. Haken and H. C. Wolf, *The Physics of Atoms and Quanta* (Springer-Verlag, Berlin, 1993).

[3] Y. G. Semenov and S. M. Ryabchenko, Effects of photoluminescence polarization in semiconductor quantum wells subjected to an in-plane magnetic field, Phys. Rev. B **68**, 045322 (2003).

[4] Y. G. Kusrayev, A. V. Koudinov, I. G. Aksyanov, B. P. Zakharchenya, T. Wojtowicz, G. Karczewski, and J. Kossut, Extreme In-Plane Anisotropy of the Heavy-Hole $g$ Factor in (001)-CdTe/CdMnTe Quantum Wells, Phys. Rev. Lett. **82**, 3176 (1999).

[5] A. V. Koudinov, I. A. Akimov, Y. G. Kusrayev, and F. Henneberger, Optical and magnetic anisotropies of the hole states in Stranski-Krastanov quantum dots, Phys. Rev. B **70**, 241305 (2004).

[6] A. Bogucki, T. Smoleński, M. Goryca, T. Kazimierczuk, J. Kobak, W. Pacuski, P. Wojnar, and P. Kossacki, Anisotropy of in-plane hole $g$ factor in CdTe/ZnTe quantum dots, Phys. Rev. B **93**, 235410 (2016).

[7] A. A. Sirenko, T. Ruf, M. Cardona, D. R. Yakovlev, W. Ossau, A. Waag, and G. Landwehr, Electron and hole $g$ factors measured by spin-flip Raman scattering in CdTe/$Cd_{1-x}Mg_xTe$ single quantum wells, Phys. Rev. B **56**, 2114 (1997).

[8] Y. G. Kusrayev, A. V. Koudinov, D. Wolverson, and J. Kossut, Anisotropy of spin-flip Raman scattering in CdTe/CdMnTe quantum wells, Phys. Status Solidi B **229**, 741 (2002).

[9] A. V. Koudinov, N. S. Averkiev, Y. G. Kusrayev, B. R. Namozov, B. P. Zakharchenya, D. Wolverson, J. J. Davies, T. Wojtowicz, G. Karczewski, and J. Kossut, Linear polarization of the photoluminescence of quantum wells subject to in-plane magnetic fields, Phys. Rev. B **74**, 195338 (2006).

[10] J. Debus, D. Dunker, V. F. Sapega, D. R. Yakovlev, G. Karczewski, T. Wojtowicz, J. Kossut, and M. Bayer, Spin-flip Raman scattering of the neutral and charged excitons confined in a CdTe/(Cd, Mg)Te quantum well, Phys. Rev. B **87**, 205316 (2013).

[11] R. Dahbashi, J. Hübner, F. Berski, K. Pierz, and M. Oestreich, Optical Spin Noise of a Single Hole Spin Localized in an (In, Ga)As Quantum Dot, Phys. Rev. Lett. **112**, 156601 (2014).

[12] M. Syperek, D. R. Yakovlev, A. Greilich, J. Misiewicz, M. Bayer, D. Reuter, and A. D. Wieck, Spin Coherence of Holes in GaAs/(Al, Ga)As Quantum Wells, Phys. Rev. Lett. **99**, 187401 (2007).

[13] E. A. Zhukov, D. R. Yakovlev, A. Schwan, O. A. Yugov, A. Waag, L. W. Molenkamp, and M. Bayer, Spin coherence of electrons and holes in ZnSe-based quantum wells studied by pump-probe Kerr rotation, Phys. Status Solidi B **251**, 1872 (2014).

[14] C. Gradl, M. Kempf, D. Schuh, D. Bougeard, R. Winkler, C. Schüller, and T. Korn, Hole-spin dynamics and hole $g$-factor anisotropy in coupled quantum well systems, Phys. Rev. B **90**, 165439 (2014).

[15] V. V. Belykh, D. R. Yakovlev, J. J. Schindler, E. A. Zhukov, M. A. Semina, M. Yacob, J. P. Reithmaier, M. Benyoucef, and M. Bayer, Large anisotropy of electron and hole $g$ factors in infrared-emitting InAs/InAlGaAs self-assembled quantum dots, Phys. Rev. B **93**, 125302 (2016).

[16] N. Allen and J. H. Eberly, *Optical Resonance and Two-Level Atoms* (Wiley, New York, 1975).

[17] V. N. Lisin, A. M. Shegeda, and K. I. Gerasimov, Oscillations of the photon echo intensity in a pulsed magnetic field: Zeeman splitting in $LiLuF_4 : Er^{3+}$, JETP Lett. **95**, 61 (2012).

[18] L. Langer, S. V. Poltavtsev, I. A. Yugova, D. R. Yakovlev, G. Karczewski, T. Wojtowicz, J. Kossut, I. A. Akimov, and M. Bayer, Magnetic-Field Control of Photon Echo from the Electron-Trion System in a CdTe quantum well: Shuffling Coherence between Optically Accessible and Inaccessible States, Phys. Rev. Lett. **109**, 157403 (2012).

[19] S. V. Poltavtsev, I. A. Yugova, Y. A. Babenko, I. A. Akimov, D. R. Yakovlev, G. Karczewski, S. Chusnutdinow, T. Wojtowicz, and M. Bayer, Quantum beats in the polarization of the spin-dependent photon echo from donor-bound excitons in

CdTe/(Cd, Mg)Te quantum wells, Phys. Rev. B **101**, 081409(R) (2020).

[20] G. L. Bir and G. E. Pikus, *Symmetry and Strain-Induced Effects in Semiconductors* (Wiley, New York, 1974).

[21] X. Marie, T. Amand, P. Le Jeune, M. Paillard, P. Renucci, L. E. Golub, V. D. Dymnikov, and E. L. Ivchenko, Hole spin quantum beats in quantum-well structures, Phys. Rev. B **60**, 5811 (1999).

[22] T. Kiessling, A. V. Platonov, G. V. Astakhov, T. Slobodskyy, S. Mahapatra, W. Ossau, G. Schmidt, K. Brunner, and L. W. Molenkamp, Anomalous in-plane magneto-optical anisotropy of self-assembled quantum dots, Phys. Rev. B **74**, 041301 (2006).

[23] D. N. Krizhanovskii, A. Ebbens, A. I. Tartakovskii, F. Pulizzi, T. Wright, M. S. Skolnick, and M. Hopkinson, Individual neutral and charged $In_xGa_{1-x}As$-GaAs quantum dots with strong in-plane optical anisotropy, Phys. Rev. B **72**, 161312 (2005).

[24] S. V. Poltavtsev, Y. V. Kapitonov, I. A. Yugova, I. A. Akimov, D. R. Yakovlev, G. Karczewski, M. Wiater, T. Wojtowicz, and M. Bayer, Polarimetry of photon echo on charged and neutral excitons in semiconductor quantum wells, Sci. Rep. **9**, 5666 (2019).

[25] S. V. Poltavtsev, M. Reichelt, I. A. Akimov, G. Karczewski, M. Wiater, T. Wojtowicz, D. R. Yakovlev, T. Meier, and M. Bayer, Damping of Rabi oscillations in intensity-dependent photon echoes from exciton complexes in a CdTe/(Cd, Mg)Te single quantum well, Phys. Rev. B **96**, 075306 (2017).

[26] M. Salewski, S. V. Poltavtsev, I. A. Yugova, G. Karczewski, M. Wiater, T. Wojtowicz, D. R. Yakovlev, I. A. Akimov, T. Meier, and M. Bayer, High-Resolution Two-Dimensional Optical Spectroscopy of Electron Spins, Phys. Rev. X **7**, 031030 (2017).

[27] S. V. Poltavtsev, I. A. Yugova, I. A. Akimov, D. R. Yakovlev, and M. Bayer, Photon echo from localized excitons in semiconductor nanostructures, Phys. Solid State **60**, 1635 (2018).

[28] F. Saeed, M. Kuhnert, I. A. Akimov, V. L. Korenev, G. Karczewski, M. Wiater, T. Wojtowicz, A. Ali, A. S. Bhatti, D. R. Yakovlev, and M. Bayer, Single-beam optical measurement of spin dynamics in CdTe/(Cd, Mg)Te quantum wells, Phys. Rev. B **98**, 075308 (2018).

[29] G. Garcia-Arellano, F. Bernardot, G. Karczewski, C. Testelin, and M. Chamarro, Spin relaxation time of donor-bound electrons in a CdTe quantum well, Phys. Rev. B **99**, 235301 (2019).

[30] P. Lawaetz, Valence-band parameters in cubic semiconductors, Phys. Rev. B **4**, 3460 (1971).

[31] A. A. Kiselev, K. W. Kim, and E. Yablonovitch, In-plane light-hole $g$ factor in strained cubic heterostructures, Phys. Rev. B **64**, 125303 (2001).

[32] M. V. Durnev, M. M. Glazov, and E. L. Ivchenko, Giant Zeeman splitting of light holes in GaAs/AlGaAs quantum wells, Phys. E **44**, 797 (2012).

[33] S. Glasberg, H. Shtrikman, I. Bar-Joseph, and P. C. Klipstein, Exciton exchange splitting in wide GaAs quantum wells, Phys. Rev. B **60**, R16295(R) (1999).

[34] E. L. Ivchenko, *Optical Spectroscopy of Semiconductor Nanostructures* (Alpha Science, Harrow, 2005).

[35] I. A. Yugova, M. M. Glazov, E. L. Ivchenko, and A. L. Efros, Pump-probe Faraday rotation and ellipticity in an ensemble of singly charged quantum dots, Phys. Rev. B **80**, 104436 (2009).